

# Disturbance observer based sliding mode control of a fabric based soft arm segment: compliant interaction with the continuum

Zhi Qiao, Pham H. Nguyen and Wenlong Zhang \*

add a more overall statement of why control of soft arm is important.

Abstract fabric continuum soft robotic arm

This work tackles for the first time the development of the augmented rigid arm model and compliant motion controller for a fabric based soft arm segment. We introduce a new parameter to the conventional augmented rigid arm model to describe the dynamics of the soft arm planetary motion. The controller is designed to estimate lumped disturbance of the soft arm and stay compliant to the unstructured environment. The validity of the controller is proven analytically. The controller and two other benchmark controllers are evaluated through experiments on a fabric soft robot. → add what conclusions from data

**Keywords:** Sliding mode control, Nonlinear disturbance observer, Soft robotics

## 1. Introduction

Where rigid manipulators highlight their capabilities to perform precise repeated motions within a known setting, they face limitations when working in an unknown and unstructured environment due to their rigid design. Therefore, soft robotics has recently emerged as a possible bio-inspired solution to create intrinsically soft robots in nature. Soft robots can embody intelligence with their compliant nature, much like their biological counterparts, like octopus limbs and elephant trunks. Their inherent compliance makes them also safe with human-robot interaction.<sup>1</sup>

The fluid-based and cable-driven mechanism has been widely utilized in the design of soft robots. A fluid-based actuator has shown a higher power-to-weight ratio and lower fabrication price than the cable-driven actuator. The fluid-based actuator can be subdivided based on the type of soft materials, including pneumatic artificial muscles (PAMs),<sup>2,3</sup> elastomeric,<sup>4,5</sup> and inflatable-fabric<sup>6,7</sup> based actuators. The structure stiffness, interaction performance, and other dynamic behaviors of the soft robots are also affected by different soft

materials. Compared with PAMs and elastomeric actuators, the fabric-based actuator shows lower structural stiffness and weight. These advantages of fabric-based actuators also imply great potentials in wearable applications or tasks requiring compliant interaction. However, the low structural stiffness also makes it more challenging to model the fabric-based actuator than the PAMs and elastomeric actuators. in comparison to

Excluding the effect of soft material properties, building the kinematic and dynamic model for soft robots is still a non-trivial task due to its theoretical infinite dimensionality. Constant curvature (CC) is the most commonly used assumption to describe the kinematic model of soft robot.<sup>8</sup> The CC framework reduces the infinite dimensionality of the soft robot to three degrees of freedom (DoFs), but a portion of the manipulator dynamics is also lost during the process. A series of CC sections can be connected in-line to form a piece-wise constant curvature model (PCC), which was utilized for multi-section soft manipulator.<sup>9</sup> Other researchers also explored higher DoFs models that based on beam theory,<sup>10</sup> Ritz-

\*Z. Qiao is with School for Engineering of Matter, Transport, and Energy, Arizona State University, Tempe, AZ, 8527, USA. Email: Zhi.Qiao.1@asu.edu. P. H. Nguyen and W. Zhang are with The Polytechnic School, Arizona State University, Mesa, AZ, 85212, USA. Email: nhpham2@asu.edu, Wenlong.Zhang@asu.edu.

*slightly confusing*

Galerkin theory<sup>11</sup> and Cosserat rod theory.<sup>12,13</sup> However, the increase of computational and sensing costs limited the usage of those complex models. Dynamic model based on PCC assumptions were presented in Ref.<sup>9,14</sup> The dynamic model was presented in the Euler-Lagrangian form, and potential energy due to the stiffness and damping effect was added to the framework. The augmented rigid arm dynamic model was presented in Ref.<sup>15-17</sup> The model assumed a backbone existed at the center line and created a virtual rigid robot under the PCC assumption to match the soft robot. It also enabled the application of rigid robot control strategies onto a soft robot. To the best of the author's knowledge, there has been no previous work on designing and validating the augmented rigid arm model for fabric-based soft robots without the backbone structure.

*cite*

*Xe*

Model-based dynamic control of soft manipulators is a relatively well-studied field. An augmented rigid arm model was used for trajectory tracking and interaction with the environment in Ref.<sup>15,16</sup> A proportional-derivative (PD) feedback controller was designed for trajectory tracking in curvature space, and another impedance controller was presented for surface following. A dynamic model based on PCC assumption was used for a soft arm with three segments in Ref.<sup>14</sup> A first-order sliding mode control (SMC) algorithm was used to track the trajectory in curvature space. A based nonlinear dynamic model based on a neural network was used for an inflatable-fabric humanoid robot in Ref.<sup>18</sup> A model predictive control (MPC) was combined with the dynamic model for position tracking. A second-order data-driven model was used for an inflatable soft arm in Ref.<sup>19</sup> A proportional-integral (PI) controller and an iterative learning controller (ILC) were used for fast and accurate position tracking. However, there are limited results in developing controllers for interacting with environments using the fabric-based system.

Leveraging on this work, and with the goal of making a step towards exploring compliant interaction with external environment using a fabric-based soft robot, we propose an augmented rigid arm model for a fabric-based soft robot without backbone and a sliding model control with nonlinear disturbance observer and state switching

*not sure this is correct way to do this reference*

(SMCWNDOS) algorithm for dynamic tasks. The controller aims to be robust against the model uncertainties, autonomously detect the contact with the environment, and change between different control modes to achieve compliant interaction with the environment.

This work contributes:

- the first augmented rigid arm model for a fabric-based soft robot.
- the first closed-loop dynamic controller for a fabric-based soft robot capable of being robust against model uncertainties and compliantly interacting with the environment
- validation of the controllers in experiments using the fabric-based system in Figure 1

The rest of the paper is organized as follows. The design of fabric-based soft arm together with the pneumatic-electronic parts is presented. This is followed by the dynamic model formulation, the traditional SMC controller design, the SMC with nonlinear disturbance observer design, and the SMCWNDOS controller design. The experimental setup and results with the no object and object in the path cases are presented in the following section. The conclusion and future work are presented at the last of this paper.

## 2. Materials and Methods

### 2.1. Design of the fabric-based soft arm

The fabric-based soft arm used in this paper is introduced in our previous work.<sup>20</sup> The arm consists of three segments, and each segment includes three fabric bending actuators. The fabric bending actuator contains two parts: rectangular-shaped air pillows and an inextensible fabric layer with various pockets. Each pocket holds one air pillow, and all the pillows are serially connected. When the bending actuator is inflated, the pillows in the pockets start interacting and then creating a bending motion. The interactions between the small pillows are difficult to predict which brings more uncertainties to the model and controller design.

[Figure 1 about here.]

*Need to clearly state how this work differs from Mathias Hofer's work from ETH Zurich*

## 2.2. System

Please  
draw  
a 2D sketch

The whole system setup is presented in Fig. 1. Two Raspberry Pi 3B are utilized individually as the controller for high-level and low-level loops in the system. The high-level loop reads the position feedback from the motion capture system (Optitrack) at 120Hz and generates desired pressure profiles for the low-level loop. The low-level loop contains three pressure regulators, one ADC board, one I2C multiplexer, and three DAC boards. Once the pressure profile is received, the low-level controller converts the pressure signal to a voltage signal through the DAC board and sends it to the regulator. The regulator adjusts the air pressure based on the input signal while the air pressure measurement is converted to a digital signal through the ADC board and collected by the low-level controller. The multiplexer is utilized to resolve the DAC address conflation.

### 2.2. Dynamic model of fabric-based robots with uncertainties

The augmented rigid-arm model for soft robotics is first proposed in<sup>16</sup> for an elastomeric-based actuator. The proposed approach follows the PCC assumption and hypothesis that the inextensible arc is located at the geometric center of the actuator.<sup>21</sup> However, the inextensible arc for our fabric-based is designed in a triangular shape, shown in Fig 2(a). When inflated to different pressure values, the inextensible arc will move along the edge of the triangle. We also assume the arc is located at the geometric center when the three chambers are inflated to the same pressure.

[Figure 2 about here.]

The orientation of the segment  $i$  is described by two parameters  $\psi_i \in [0, 2\pi]$  and  $\theta_i \in [-\frac{\pi}{2}, +\frac{\pi}{2}]$ .  $\psi_i$  and  $\theta_i$  indicates the counterclockwise rotation angle with respect to axis  $s_{i-1}$  and  $n_{i-1}$ , respectively. The origins  $O_{i-1}$  and  $O_i$  are placed at the center of the bottom and top plates. Axis  $s$  is perpendicular to its local plate and axis  $o$  goes through the connection point between chamber 2 and 3. Since the actuator is not designed for twisting motion, we only focus on tracking the bending angle  $\theta_i$  and the configuration of the soft arm segment is described by  $q_i = \theta_i$ . For simplicity, we refer  $q_i$  as  $q$  in the rest of the paper.

In order to match the design of the fabric-based soft actuator, we introduced a new parameter  $r_i$  into the augmented robot model, as shown in Fig.2(c).  $r_i$  reflects the distance between the center line and the inextensible arc with length  $L_i$  and it is estimated based on the position of the segment's top center point  $[x_{ti}, y_{ti}]^T$  in its base frame  $O_{i-1}$  as follows:

$$\phi = \tan(\frac{y_{ti}}{x_{ti}})$$

$$r_i = \frac{l_{rect}}{\sqrt{3}} \frac{\cos(\pi/3)}{\cos((\phi \bmod 2\pi/3) - \pi/3)} \quad (1)$$

where  $l_{rect}$  is the length of one side of the triangle.

The Denavit-Hartenberg (DH) parameters for the augmented robot presented in Fig. 2(b) is listed in TABLE 1. The configuration of the augmented robot is described by joint space vector  $\gamma_i = [\frac{\theta_i}{2}, b_i(\theta_i), b_i(\theta_i), \frac{\theta_i}{2}]^T$  where  $b_i(\theta_i)$  is calculated as follows:

$$b_i(\theta_i) = (\frac{L_i}{\theta_i} - \text{sign}(\theta_i)r_i)\sin(\frac{\theta_i}{2}) \quad (2)$$

[Table 1 about here.]

Following the derivation presented in Ref.<sup>16</sup> a projection between augmented rigid robot joint space and soft arm segment joint space is presented as follows:

$$J_\gamma(q) = \frac{\partial \gamma}{\partial q} = [\frac{1}{2}, h(\theta), h(\theta), \frac{1}{2}]^T \quad (3)$$

where  $h(\theta) = \frac{1}{2}(\frac{L_i}{\theta_i} - r_i)\cos(\frac{\theta_i}{2}) - \frac{L_i}{\theta_i}\sin(\frac{\theta_i}{2})$  and the dynamics for the soft arm is:

$$M(q)\ddot{q} + C(q, \dot{q})\dot{q} + G(q) = \tau + \tau_{ext} \quad (4)$$

$$\tau_{ext} = J^T(q)f_{ext}$$

where  $M, C, G$  are the inertia term, centrifugal and Coriolis term and the gravity term.  $J^T(q)$  projects the external force  $f_{ext}$  to the soft robot joint torque. In this work, we assume the segment is actuated by two internal torques the axes  $x$  and  $y$ . Based on the geometric parameter the internal torques are calculated as follows:

$$\begin{bmatrix} \tau_x \\ \tau_y \end{bmatrix} = \alpha \begin{bmatrix} -\sin(\frac{\pi}{6}) & -\sin(\frac{\pi}{6}) & 1 \\ \cos(\frac{\pi}{6}) & -\cos(\frac{\pi}{6}) & 0 \end{bmatrix} p_i \quad (5)$$

where  $p_i = [p_{m1i}, p_{m2i}, p_{m3i}]$  is the chamber pressure vector for segment  $i$ .  $\alpha$  is an amplifying coefficient and its identification process is detailed in

the following section. Considering the soft robot configuration, the resulting joint torque is:

$$\begin{aligned} \tau_i &= [\sin\psi \ - \cos\psi] \cdot [\tau_x, \tau_y]^T \\ &= \alpha R(\psi) p_i \end{aligned} \quad (6)$$

We introduce the stiffness and damping terms to complete Eq. 4 as follows:

$$\begin{aligned} M(q)\ddot{q} + C(q, \dot{q})\dot{q} + G(q) + Kq + D\dot{q} \\ = \alpha R(\psi)p + \tau_{ext} \end{aligned} \quad (7)$$

### 2.3. Design of Sliding Mode Controller(SMC)

Considering the model uncertainties, we rephrase Eq. 7 for segment  $i$  as follows:

$$\begin{aligned} m(q)\ddot{q} + c(q, \dot{q})\dot{q} + g(q) + \hat{k}q + \hat{d}\dot{q} &= \hat{\alpha}R(\psi)p, \\ \hat{k} &= k_0 + \Delta k, \\ \hat{d} &= d_0 + \Delta d, \\ \hat{\alpha} &= (1 + \Delta\alpha)\alpha_0 \end{aligned} \quad (8)$$

where  $|\Delta k| < K_m$ ,  $|\Delta d| < D_m$ , and  $|\Delta\alpha| < \alpha_m$  denote the parameter bounded uncertainties.

We rewrite the model in state-space form as:

$$\begin{aligned} \dot{x}_1 &= x_2, \\ \dot{x}_2 &= f(x_1, x_2) + \frac{\alpha_0}{m(x_1)}u + \Delta, \\ f(x_1, x_2) &= -m(x_1)^{-1}((c(x_1, x_2) + d_0)x_2 \\ &\quad + k_0x_1 + g(x_1)), \\ \Delta &= -\Delta k \frac{x_1}{m(x_1)} - \Delta d \frac{x_2}{m(x_1)} \\ &\quad + \Delta\alpha \frac{\alpha_0}{m(x_1)} + \tau_{ext} \\ u &= R(\psi)p \end{aligned} \quad (9)$$

where  $|\tau_{ext}| < \tau_m$  denotes the bounded external torque.

The tracking error for the system is described as  $e = x_1 - x_{d1}$  and the switching surface and its differential are:

$$\sigma = \dot{e} + \lambda e, \lambda > 0 \quad (10)$$

$$\dot{\sigma} = \ddot{e} + \lambda\dot{e} \quad (11)$$

Substituting Eq. 9 into Eq. 11 yields

$$\begin{aligned} \dot{\sigma} &= \lambda\dot{e} + \ddot{e} = \lambda\dot{e} + \ddot{x}_1 - \ddot{x}_{d1} \\ &= \lambda\dot{e} - \ddot{x}_{d1} + f(x_1, x_2) + \frac{\alpha_0}{m(x_1)}u + \Delta \end{aligned} \quad (12)$$

The reaching law is presented as:

$$\dot{\sigma} = -\eta \text{sign}(\sigma) \quad (13)$$

The sliding surface Eq. 10 and the reaching law Eq. 13 the control input is designed as:

$$\begin{aligned} u &= \frac{m(x_1)}{\alpha_0}(\ddot{x}_{d1} - \lambda\dot{e} - f(x_1, x_2) - \eta \text{sign}(\sigma)), \\ \eta &\geq \frac{1}{1 + \alpha_m}(\alpha_m|\lambda\dot{e} - \ddot{x}_{d1} + f(x_1, x_2)| \\ &\quad + |\frac{K_m x_1}{m(x_1)}| + |\frac{D_m x_2}{m(x_1)}| + |\frac{\tau_m}{m(x_1)}| + \epsilon) \end{aligned} \quad (14)$$

where  $\epsilon$  is positive number. Selecting a larger  $\eta$  drives the system to the sliding surface faster with a sacrifice of more shattering. The stability proof is presented in Appendix A

### 2.4. Design of the sliding mode control with nonlinear disturbance observer(SMCNDO)

The control input  $u$  is rewrite as:

$$\begin{aligned} u &= u_{eq} + u_s + u_n \\ u_{eq} &= -b(x_1)^{-1}(f(x_1, x_2) + \lambda\dot{e} - \ddot{x}_d + k_{sf}\sigma), \\ u_n &= -b(x_1)^{-1}\hat{\Delta}, \\ u_s &= -b(x_1)^{-1}\eta \text{sat}(\sigma), \\ \text{sat}(\sigma) &= \begin{cases} \text{sign}(\sigma) & |\sigma| > \mu \\ \frac{\sigma}{\mu} & |\sigma| \leq \mu \end{cases} \end{aligned} \quad (15)$$

where  $\hat{\Delta}$  is the estimation of the lumped disturbance.  $\eta$  and  $\mu$  are positive constant and selected by the user. Substituting into Eq.(12):

$$\begin{aligned} \dot{\sigma} &= -k_{sf}\sigma - \eta \text{sat}(\sigma) + \bar{\Delta}, \\ \bar{\Delta} &= \Delta - \hat{\Delta} \end{aligned} \quad (16)$$

This indicates the if the disturbance estimation error  $\bar{\Delta}$  goes zero, the system tracking error will also go zero.

In order to estimate the lumped disturbance  $\Delta$  in realtime, a modified disturbance observer from Ref<sup>22</sup> is designed as follows:

$$\begin{aligned} \hat{\Delta} &= \hat{z} + w(\sigma), \\ \dot{\hat{\Delta}} &= \dot{\hat{z}} + \frac{\partial w}{\partial \sigma} \dot{\sigma} \end{aligned} \quad (17)$$

We choose  $w(\sigma) = k_w \sigma, k_w > 0$  and substitute with Eq.12

$$\dot{\Delta} = \dot{z} + k_w(b(x_1)u_n + b(x_1)u_s + \Delta) \quad (18)$$

The update law for  $\dot{z}$  is selected as:

$$\dot{z} = -k_w(b(x_1)u_n + b(x_1)u_s + \Delta) \quad (19)$$

Assuming  $\dot{\Delta}$  is bounded and plugging into Eq. (18):

$$\begin{aligned}\dot{\Delta} &= k_w \bar{\Delta}, \\ \dot{\bar{\Delta}} &= -k_w \bar{\Delta} + \dot{\Delta},\end{aligned}\quad (20)$$

This suggests that  $\bar{\Delta}$  is stable and the estimation error is bounded.

### 2.5. Soft contact with SMCWNDOS

When the soft arm contacts the environment, we assumed that the external load would be dominant. A three-state switching framework is introduced in this work to ensure the system can detect the contact event, maintain compliance during the contact, and recover to the original desired path after the contact. We assume that 1) the system always starts with no contact with the object. 2) The object's stiffness is higher than the system, and the object stays stationary during the contact. The three states include Normal mode, Compliant mode, and Recovery mode, whose switching conditions are presented in Fig. 3. The system starts and stays within the normal mode to track the original desired path until the estimated lumped disturbance, and the tracking error goes beyond the thresholds ( $\epsilon_{th1}$  and  $\Delta_{th1}$ ). Once switched to the compliant mode, the system augments its desired path temporally to its current position to avoid the over-estimation of the lumped disturbance. When the estimated disturbance reduces below the threshold  $\Delta_{th2}$ , the system will switch to recovery mode to reach the original desired path. A ramp reference will be calculated in recovery mode based on the current position and the original desired path to avoid false detection during the recovery mode. If the lumped disturbance is above the threshold value, it indicates the object is not moved out, and the system will step back to the compliant mode.

[Figure 3 about here.]

*rework*

w +

What is this acceptable ness? (expand & explain 5)

### 3. Results

The performance of the proposed augmented model is presented in Fig. 4. The tracking errors are normalized with respect to the length of the actuator. The proposed augmented model shows acceptable accuracy in all range of motion but its performance got impeded when close to perpendicular up case. This reduction of the model accuracy is due to the small chamber air pressure and the low structure stiffness of the fabric material.

[Figure 4 about here.]

*explain more*

To identify the boundary of the model parameter's uncertainties, the actuator is excited with sum of sines signals as follows:

$$u = \sum_{j=1}^{10} Amp * \sin(2\pi f_j t + \phi_j) + b_{off} \quad (21)$$

where  $Amp = 1.25$  and  $b_{off} = 1.25$  are selected to ensure input  $u$  stay within the operational range. Ten different frequency components  $f_j$  are evenly selected from [0.001, 0.1] Hz and phase constant  $\phi_j \in [0, 2\pi]$  is randomly selected. The time interval for each trial is sixty seconds and nine trials are collected in total. All parameters are evaluated by MATLAB grey-box estimation toolbox with *lsqnonlin* algorithm and the results are presented in Fig. 5 where  $k_0 = 0.4897, d_0 = 0.8616, \alpha_0 = 1.2634$  and  $\Delta k = 0.4345, \Delta d = 0.6600, \Delta \alpha = 1.0183$ .

[Figure 5 about here.]

*all 3?*

Two experiments are designed to evaluate the performance of the proposed control framework. In all experimental cases, the actuator is pre-inflated to 1 psi to ensure the starting point close to the same position. A trapezoid path is then designed to bend 15 degrees from the starting point with a ramp rate of 1 deg/s. In the first scenario, no object is placed in the middle of the path while, in the second case, an object (wooden plate) is placed at the marked position until 22 secs after the trial starts.

[Figure 6 about here.]

*why 22 secs*

how well?  
percentage?  
This means  
short video sequence  
(video screenshots)

figure?

The experiment results for the first scenario in Fig. 6. Clips of video from SMCWN DOS method is presented in Fig. 6(a). The experimental results for the conventional SMC algorithm are shown Fig. 7(b) and (c). The SMC method can track the original path but the oscillation is also observed. The results of the proposed algorithm are depicted Fig. 7(d), (e) and (f). The algorithm can track the trapezoid signal with less oscillation and the maximum value of the estimated lumped disturbance is below  $0.5 \text{ N} \cdot \text{m}$ .

what is  
2nd scenario

how  
high?

The experiment results for the second scenario in Fig. 7. Clips of video from SMCWN DOS method is presented in Fig. 6(a). Fig. 7(b) and (c) presents the results from the traditional SMC controller. The traditional SMC method can still track the original path after the object is removed. However, high air pressure is also observed during the contact, indicating the soft robot is not compliant with the object. Fig. 7(d), (e) and (f) presents the results of the baseline SMCNDO algorithm. The baseline algorithm can barely track the desired path after the object is removed. During the contact phase, the actuator cannot fully reject the lumped disturbance, leading to a large increase in the estimated disturbance. This accumulation also makes the system oscillating after the contact. The results of the SMCWN DOS algorithm with object is presented in Fig. 7(g), (h) and (i). It is observed that the oscillation is reduced after the object is removed, and the estimated disturbance for the augmented path stop accumulates after the switch to the compliant mode.

[Figure 7 about here.]

The performance of the controllers are evaluated through two criteria: the normalized chamber air pressure (NP) during the contact and the absolute value of maximum position overshoot (MPO) after the contact. The former one reflects the level of compliance during the contact and the chamber pressure is normalized with respect to the hardware limit. The latter one reflects the level of aggressiveness after the contact. The evaluation results are listed in TABLE 2. The proposed SMCWN DOS algorithm over-performs the other two controllers in both criteria. The proposed controller shows significantly reduction in the chamber air pressure during the contact while both the

competitors gets closed to the maximum air pressure. Both the SMC and SMCNDO method assumes the system is powerful enough to reject the lumped disturbance but they all get saturated due to the hardware limit. For SMCNDO method, the saturation also leads to the over-estimation of the lumped disturbance. The proposed controller augments desired path during the contact to resolve the overestimation. The smallest MPO value is also observed for the proposed controller while the SMCNDO method shows the largest MPO value. The main reason behind the performance difference is still the overestimation of the lumped disturbance. Due to the overestimation, the SMCNDO controller requires longer time to correct the estimation and fails to recover to the original path within the time limit.

what  
is barely?

[Table 2 about here.]

what is it?  
repeat here

#### 4. Conclusion

We proposed a modified augmented rigid arm model and a SMCWN DOS algorithm for a fabric-based soft arm segment in this work. A new model parameter  $r_f$  was introduced to improve the model accuracy. The uncertainties of the model parameters were identified by exciting the system with a sum of sine signals. A three-state switching algorithm was presented to improve the tracking performance. The stability of the SMCWN DOS algorithm was proved to be ultimately bounded in the sense of Corless and Leitmann. The baseline experiment and the experiment with contacting the object indicated that the SMCWN DOS algorithm could detect the contact, augment the desired path, recover to the original desired path. The small values of NP and MPO indicated that SMCWN DOS controller is more compliant during the contact and less aggressive after the contact in comparison to the conventional SMC and the SMCNDO method.

Future studies include expanding the SMCWN DOS framework to higher DOFs, improving the performance by adding more deflation sources, investigating the motion planning strategy to control the soft robotic arm with multi-segment.

describe hardware limit.



Figure 1. System Overview.

DRAW IT ↗

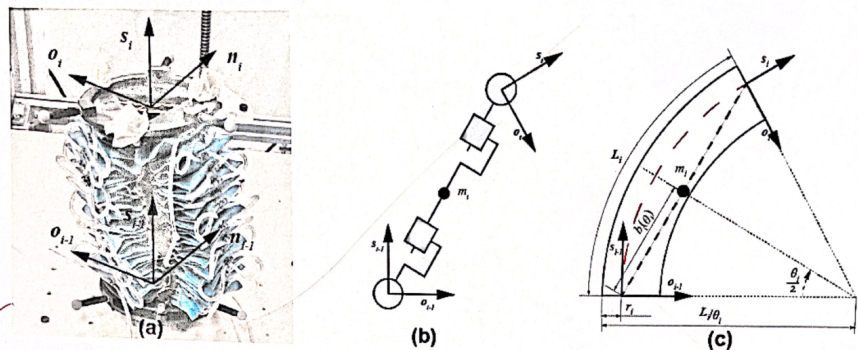


**Figure 2.** Modified augmented rigid arm model for a single segment.(a) Isometric view of the segment;(b) Augmented robot (RPPR);(c) Modified model with addition of parameter  $r_i$ . The blue, black and red lines indicate the top and bottom plates, the inextensible layer and the geometric center line, respectively.

does  
not highlight triangularity

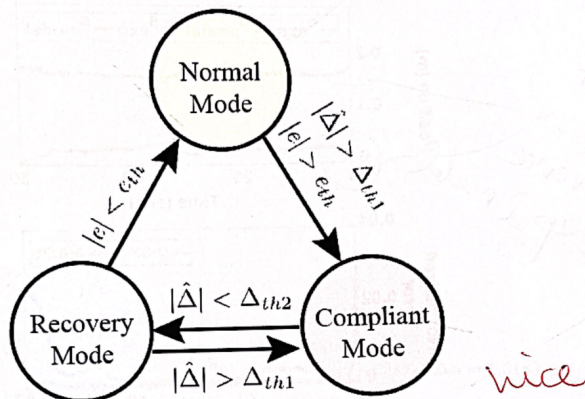


**Figure 3.** Three-state control framework for soft contact using SMCWNDOS. The system always starts from normal mode and will switch to compliant mode when both position error and estimated disturbance goes above the threshold.  $\Delta_{th2} < \Delta_{th1}$  allows the soft arm autonomously switch to recovery mode when the estimated disturbance is small enough and return from recovery mode to compliant mode if the estimated disturbance is too large.

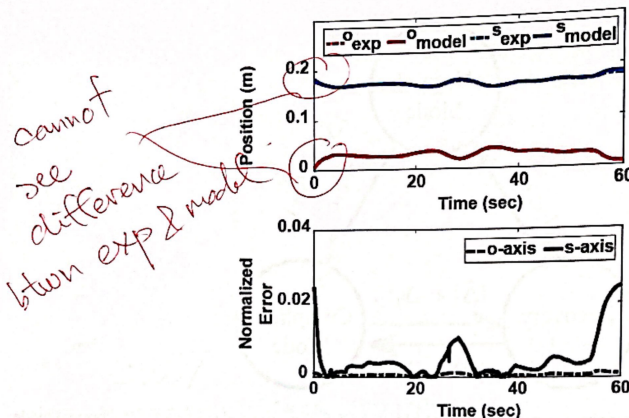


**Figure 4.** Experimental results for the proposed augmented model.  $o_{exp}$  and  $s_{exp}$  is the experimental result on  $o$  and  $s$  axis, respectively.  $o_{model}$  and  $s_{model}$  is the model prediction result  $o$  and  $s$  axis. The error between the experimental results and model predictions are normalized with respect to the actuator length.

clean background / blur background

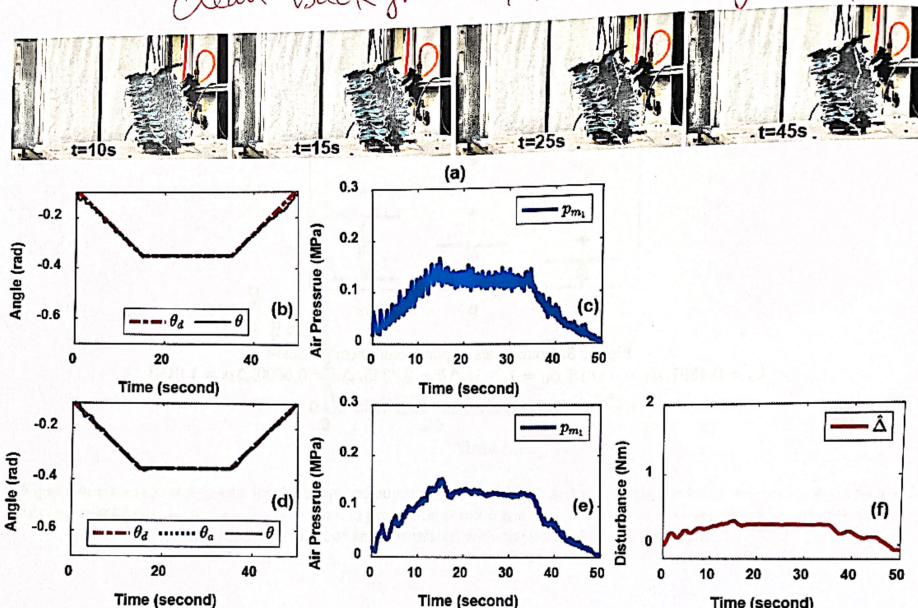


**Figure 6.** Experiments with an object.(a) clips of video from SMCWNDOS method. (b) and (c) is the position tracking and measured pressure for traditional SMC.(d), (e) and (f) is the position tracking, measured pressure and estimated disturbance for SMCWNDOS where  $\theta, \theta_d, \theta_a$  are the actual(solid black), the desired (dash-dotted red)and the augmented (dotted blue) bending angles respectively.

clean/blur background

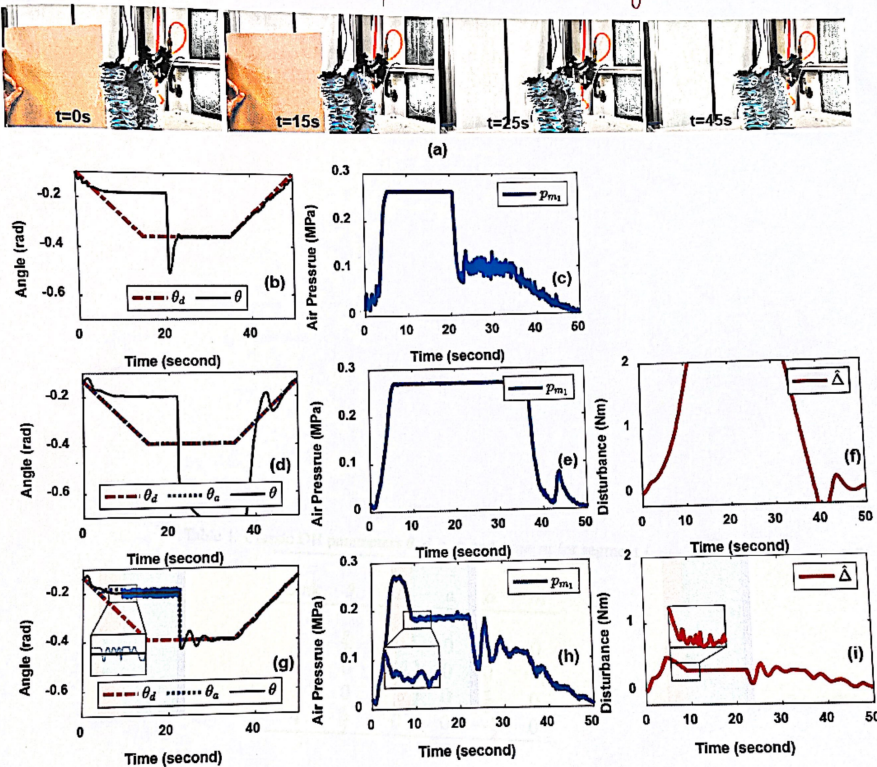


Figure 7. Experiments for object in the place. (a) and (b) are the results for SMC method. (c),(d) and (e) are the results for SMCNDO method. (f),(g),(h) and (i) are the results for SMCWNDOS method.  $\theta, \theta_d, \theta_a$  are the actual (solid black), the desired (dash-dotted red) and the augmented (dotted blue) bending angles respectively. light green, red and blue indicates the normal, compliant and recovery mode, respectively. light purple indicates the autonomous switch between the compliant and recovery mode.